Reconciling Theories for Human and Natural Attribution of Recent East Africa Drying

ANDREW HOELL AND MARTIN HOERLING

Physical Sciences Division, NOAA/Earth System Research Laboratory, Boulder, Colorado

JON EISCHEID, XIAO-WEI QUAN, AND BRANT LIEBMANN

Cooperative Institute for Research in Environmental Sciences, University of Colorado Boulder, and Physical Sciences Division, NOAA/Earth System Research Laboratory, Boulder, Colorado

(Manuscript received 27 July 2016, in final form 22 November 2016)

ABSTRACT

Two theories for observed East Africa drying trends during March–May 1979–2013 are reconciled. Both hypothesize that variations in tropical sea surface temperatures (SSTs) caused East Africa drying. The first invokes a mainly human cause resulting from sensitivity to secular warming of Indo–western Pacific SSTs. The second invokes a mainly natural cause resulting from sensitivity to a strong articulation of ENSO-like Pacific decadal variability involving warming of the western Pacific and cooling of the central Pacific. Historical atmospheric model simulations indicate that observed SST variations contributed significantly to the East Africa drying trend during March–May 1979–2013. By contrast, historical coupled model simulations suggest that external radiative forcing alone, including the ocean's response to that forcing, did not contribute significantly to East Africa drying. Recognizing that the observed SST variations involved a commingling of natural and anthropogenic effects, this study diagnosed how East African rainfall sensitivity was conditionally dependent on the interplay of those factors. East African rainfall trends in historical coupled models were intercompared between two composites of ENSO-like decadal variability, one operating in the early twentieth century before appreciable global warming and the other in the early twenty-first century of strong global warming. The authors find the coaction of global warming with ENSO-like decadal variability can significantly enhance 35-yr East Africa drying trends relative to when the natural mode of ocean variability acts alone. A human-induced change via its interplay with an extreme articulation of natural variability may thus have been key to Africa drying; however, these results are speculative owing to differences among two independent suites of coupled model ensembles.

1. Introduction

East Africa, defined herein as the land area bounded by 2.5°S–10°N and 35°–50°E (Fig. 1b, red box), a region that includes Kenya, southern Ethiopia, and Somalia, receives the majority of its precipitation during two seasons—the ''long rains'' of March–May and the ''short rains'' of October–December (Fig. 2; see also Liebmann et al. 2012). During March–May 1979–2013, a statistically significant downward trend in East African precipitation was observed (Fig. 1b; see also Verdin et al. 2005; Funk et al. 2015a) that was greater than one standard deviation from the mean of 35-yr trends during 1901–2013 (Fig. 1c).

Two temporal regimes characterize the time series of March–May East African rainfall since the late 1970s (Fig. 3). One regime experienced mostly wet conditions during 1975–89 and the second mostly dry conditions during 1990–2013. During 1990–2013, only seven March–May seasons received rainfall greater than the 1901–2013 average, suggestive of a steplike change in rainfall behavior as described by Lyon et al. (2014). End-point sensitivity of the March–May precipitation trend should also be recognized, with the magnitude of the overall drying trend during 1979–2013 enhanced by the single extremely wet 1981 in the early part of the record. Nonetheless, East African dryness since the early 1990s is likely the most extreme and prolonged dry period of the instrumental record [Fig. 3b; see also Fig. 1 of Lyon and DeWitt (2012) and Fig. 3 of Funk et al. (2015a)].

Corresponding author e-mail: Andrew Hoell, andrew.hoell@noaa.gov

DOI: 10.1175/JCLI-D-16-0558.1

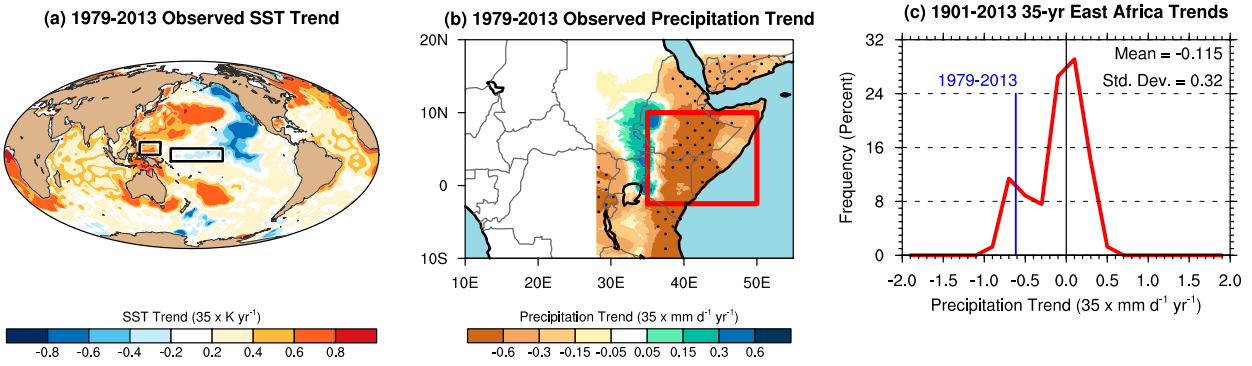

FIG. 1. (a) March–May 1979–2013 observed SST trend (shaded) and areas used to calculate the WPG (black boxes). (b) March–May 1979–2013 observed precipitation trend (shaded) where stippling denotes trends significant at $p < 0.10$ using a Student's t test. (c) PDF of 35-yr East African precipitation trends during March–May 1901–2013, with the observed 1979–2013 trend displayed in blue.

Atmospheric model simulations forced by observed time-varying boundary conditions have been studied to identify mechanisms of this observed March–May 1979–2013 East Africa drying. These experiments, referred to as the Atmospheric Model Intercomparison Project (AMIP) experiments (Gates 1992), establish that March–May 1979–2013 East African precipitation is sensitive to temporal global sea surface temperature (SST) variations, with the particular history of SST forcing (e.g., Fig. 1a) leading to a drying signal (Lyon and DeWitt 2012; Liebmann et al. 2014). The magnitude of the March–May East Africa drying occurring in the ensemble average of these experiments is weaker than the observed drying, likely consistent with the aforementioned end point issues, but the vast majority of model runs yield drying (see Liebmann et al. 2014). Currently, the relative contributions of natural internal (herein, natural) and anthropogenic sources to the observed 1979–2013 SST trend are unknown.

Two hypotheses have been proposed that give different arguments for the regional source of the SST forcing and thus point to different dominant causes of the March–May 1979–2013 East Africa drying trend. The first hypothesis, developed through a set of incremental observational analyses, has primarily centered on the idea that warming in the Indian Ocean (Williams and Funk 2011) or Indo–Pacific Ocean (Williams and Funk 2011; Funk and Hoell 2015) drives an anomalous overturning mass circulation that leads to increased subsidence and long-term drying over East Africa (see also Funk et al. 2008). The empirical approach was further developed by Williams and Funk (2011), and did not employ climate model sensitivity experiments directly. While recognizing that El Niño–Southern Oscillation has an effect on East African precipitation through modifications to the Walker circulation, Williams and Funk (2011) diagnosed the correlative behavior between warming of the Indo–western Pacific warm pool, increases in east Indian–western Pacific Ocean rainfall, and decreases in East African rainfall from which a causality chain was conjectured. Williams and Funk (2011) argue that the warm pool SST increases were anthropogenically forced through a comparison of observed SST time series and those simulated in response to radiative forcing as estimated from phase 3 of the Coupled Model Intercomparison Project (CMIP3) SST trends. Williams and Funk (2011) state that "increased Indian Ocean SSTs appear likely to continue to strongly modulate the warm pool circulation, reducing precipitation in East Africa." Williams and Funk (2011) also state that "the westward extension of MAMJ [March–June] Walker circulation appears to be partly driven by disproportionately rapid warming in the central and western Indian Ocean, which has effectively expanded the warm-pool region westward."

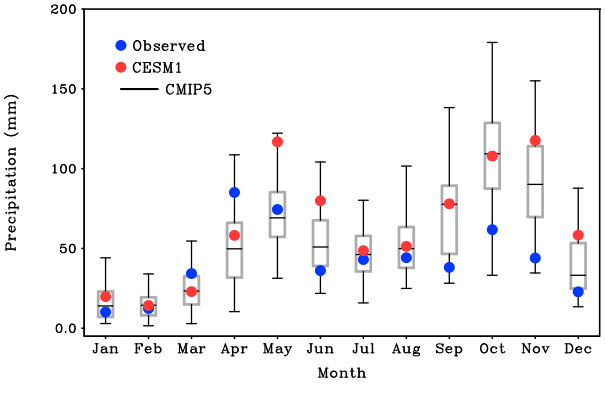

FIG. 2. Monthly average precipitation areally averaged over East Africa in observations (blue), CESM1 (red), and the CMIP5 ensemble (box-and-whisker plot).

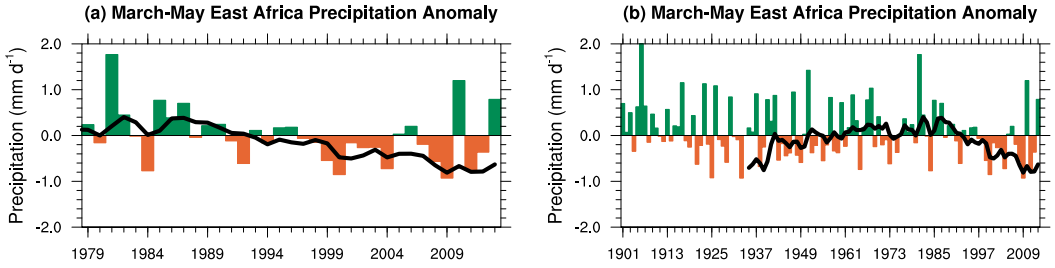

FIG. 3. East African March–May precipitation anomaly (bars) and 35-yr end-point trends (black line) for (a) 1979–2013 and (b) 1901–2013.

The argument for anthropogenically driven precipitation declines of March–May East African precipitation was revisited in Funk and Hoell (2015). Therein, a global SST trend absent effects of El Niño–Southern Oscillation was estimated from the fully forced suite of historical simulations from phase 5 of the Coupled Model Intercomparison Project (CMIP5, Taylor et al. 2012). This ''residual trend pattern,'' which highlighted a structure of enhanced SST warming over the Indo–western Pacific region relative to the east equatorial Pacific, resembled observational estimates of a residual SST change pattern since 1900 absent ENSO variability (e.g., Compo and Sardeshmukh 2010; Solomon and Newman 2012). Funk and Hoell (2015) argue, using atmospheric model simulations forced by idealized SST patterns, that this residual SST trend pattern is related to East African precipitation declines for 1979–2012. The interpretation of such a pattern of SSTs, and furthermore how it relates to the actual observed SST trend pattern during 1979–2013 (shown here in Fig. 1a), remains unclear however.

A second hypothesis, proposed by Lyon and DeWitt (2012), was based on the diagnosis of East African rainfall sensitivity in AMIP simulations using observed global SST forcing versus parallel experiments using only Pacific basin SST and Indian Ocean SST variability alone. Lyon and DeWitt (2012) state that ''the abrupt decline in long rains precipitation is linked to similarly abrupt changes in sea surface temperatures, predominately in the tropical Pacific basin.'' The result of their simulations made a compelling case for a dominant forcing originating in the tropical Pacific. Lyon (2014), Lyon et al. (2014), and Yang et al. (2014) further argued that the character of drought-producing Pacific basin SST was a mostly natural decadal variation. For example, Yang et al. (2014) state that ''the drying trend of the long rains is associated with decadal natural variability associated with sea surface temperature (SST) variations over the Pacific Ocean.'' However, the AMIP simulations of Lyon and DeWitt (2012), Lyon (2014), Lyon et al. (2014), and Yang et al. (2014) fail to quantify how much of the recent East Africa drying was attributable to human influences versus natural decadal variations since the western Pacific SST change specified in those runs undoubtedly incorporates some anthropogenic warming as argued in Funk and Hoell (2015).

To be sure, climate variability even during an overall strong global mean warming can include decadal periods of tropical Pacific cooling as a consequence of internal ocean dynamics alone (e.g., Meehl et al. 2010; Meehl and Teng 2012; Guemas et al. 2013). Further evidence supporting arguments for a natural cause of recent decadal cooling of the eastern Pacific comes from initialized decadal prediction systems that have been shown to capture a post-2000 shift to a negative interdecadal Pacific oscillation (Meehl and Teng 2012; Meehl et al. 2014).

There is a growing body of evidence that East Africa long rains were acutely sensitive to the particular SST history of 1979–2013. Liebmann et al. (2014), using a higher-resolution atmospheric model that realistically simulated East Africa's bimodal rainy seasons, also found a drying trend in their global AMIP experiments. Correlation analysis applied to their large ensemble of runs indicated particular East Africa drying sensitivity to an increased zonal SST gradient between the western Pacific and the equatorial central Pacific. Liebmann et al.'s (2014) finding provided support for the observational works by Hoell and Funk (2013, 2014) that an enhanced zonal SST gradient induces intensified convection over the Indo–western Pacific warm pool that leads to subsidence and therefore drying over East Africa. The index used to define the zonal SST gradient has been termed the western Pacific gradient (WPG) by Hoell and Funk (2013) and is calculated as the difference between areally averaged western Pacific SST (0°–10°N, 130°–150°E) and areally averaged central Pacific SST (5°S–5°N, 160°E–150°W). The WPG can also be used to identify SST patterns similar to the 1979–2013 SST trend pattern to which

East African precipitation is sensitive. The WPG is therefore an appropriate metric to identify such patterns since, by definition, it readily distinguishes SST patterns with a contrast between the west and central Pacific Oceans.

The question of an anthropogenic role in East Africa drying has received further scrutiny through a case study of the particularly severe drought year of March–May 2011. Lott et al. (2013) used an emergent modeling technique, first implemented by Pall et al. (2011), to separate natural from anthropogenic forcing of regional climate. This compares simulated East African precipitation in parallel AMIP simulations, one subjected to current climate forcings and the other without effects of human influences. Key in estimating the latter is determining the SST states that would have occurred without long-term anthropogenic influences. Estimates of these states were derived by subtracting the two SST patterns, occurring in transient coupled model simulations subjected to historical anthropogenic forcing, from those occurring in similar runs with no external forcing and then removing this difference from the 2011 observed conditions. Lott et al. (2013) provided evidence that the drought in East Africa occurring in spring 2011 was likely made more severe because of anthropogenic influences. Their results imply that either anthropogenic forcing alone or some combination of the natural SSTs in 2011 commingled with the human influence of SSTs increased drought risks. Here we will consider a similar question, though in the context of 35-yr trends in SSTs during 1979–2013. Importantly for the hypotheses being tested herein, Lott et al. (2013) found their estimate of the anthropogenic contribution to East African drought to be sensitive to the several different SST patterns derived from transient coupled models. We will thus employ two different large ensemble model datasets in our assessment, one based on a single coupled system for which a very large ensemble exists and a second derived from a very large multimodel coupled system for which each model yields a single simulation.

Section 2 describes the observed data and the various model simulations. Section 3a places the 1979–2013 East Africa drying into a longer history of that region's rainfall variability since 1901. It then assesses East African rainfall sensitivity, both to the known changes in observed external forcing alone since 1979 and to joint changes in external forcing and observed sea surface temperatures. The critical importance of the actual observed history of SST variations is established, and section 3b diagnoses composites of analogous multidecadal variations in SSTs based on historical coupled model simulations. The analysis provides insight on the intensity of the natural SST variation that occurred during 1979–2013 and also provides evidence that East Africa drying during 1979–2013 was made more likely owing to a synergy between a very strong articulation of natural interdecadal cooling in the central tropical Pacific superimposed on an overall global SST warming pattern. Section 4 provides a summary and discussion with a focus on using the results of this paper to reconcile the two theories for observed East Africa drying trends during March–May 1979–2013.

2. Observations and model simulations

a. Observed data

The four gridded observed precipitation datasets analyzed in this study are from the Global Precipitation Climatology Centre (GPCC) on a 1° × 1° grid during 1901–2013 (Becker et al. 2013), version 2 of the Climate Hazards Group Infrared Precipitation with Stations (CHIRPS) on a 0.05° × 0.05° grid during 1981–2013 (Funk et al. 2015b), the Centennial Trends Greater Horn of Africa precipitation archive (CenTrends) during 1901–2013 (Funk et al. 2015a), and the Global Precipitation Climatology Project (GPCP) on a 2.5° × 2.5° grid during 1979–2013 (Adler et al. 2003; Huffman et al. 2009). CenTrends and GPCC are constructed from station data only. GPCP is constructed from remotely sensed information and GPCC rain gauge analyses. CHIRPS is constructed from remotely sensed information, version 2 of the Climate Forecast System Reanalysis, and a rich network of station data over East Africa unique to CHIRPS and CenTrends. Only CenTrends is displayed since there is close correspondence among the four observed precipitation datasets over East Africa during their common periods of record.

The merged HadISST–OISST dataset of Hurrell et al. (2008) on a 1° × 1° grid is utilized to identify observed SST patterns and to specify the ocean boundary conditions (SST and sea ice concentrations) for the atmospheric model simulations.

b. Atmospheric model simulations

1) AMIP SIMULATIONS

Two separate AMIP ensembles are utilized. The first ensemble comprises 50 members from the Community Atmosphere Model, version 5 (CAM5; Conley et al. 2012), developed by the National Center for Atmospheric Research. The model is run at a horizontal

TABLE 1. Description of models used for AMIP simulations.

	ECHAM5.4	CAM5
Developing modeling center	Max Planck Institute for Meteorology	National Center for Atmospheric Research
Modeling center performing simulations	NOAA/ESRL	Lawrence Berkeley National Laboratory
Number of ensembles	30	50
Horizontal resolution	T159 (~0.75° × ~0.75°)	T126 (~1.0° × ~1.0°)
Levels	31	25
SST and sea ice reference	Hurrell et al. (2008)	Hurrell et al. (2008)
Greenhouse gas reference	Meinshausen et al. (2011)	Meinshausen et al. (2011)
Ozone reference	Cionni et al. (2011)	Lamarque et al. (2011)
Aerosols reference	Tanre et al. (1984)	Time varying prior to 2005, RCP6 aerosols with no volcanoes after.
Model reference	Roeckner et al. (2006)	Conley et al. (2012)

resolution of about 1° latitude/longitude and uses 30 vertical levels in the atmosphere. The second ensemble comprises 30 members from ECHAM, version 5.4 (ECHAM5.4; Roeckner et al. 2006) developed by the Max Planck Institute for Meteorology. The model is run at a horizontal resolution of about 0.7° latitude/longitude and uses 31 vertical levels in the atmosphere. Each ensemble member begins from different atmospheric initial states but is subjected to the same time-evolving specified SST, sea ice, and external radiative forcing time series for the period 1979–2013. We will focus on the 1979–2013 East African rainfall trend, for which the forced signal is derived from the ensemble mean of the AMIP simulations. We will also assess the importance of internal atmospheric variability through a diagnosis of the spread among individual AMIP simulations. A description of the atmospheric models and the boundary conditions used to drive the models are provided in Table 1. Further documentation and outputs from the atmospheric model experiments can be found online (http://www.esrl.noaa.gov/psd/repository/alias/facts).

2) RESPONSE TO VARIATIONS OF THE 1979–2013 SST TREND PATTERN

ECHAM5.4 is used to test the atmospheric response to variations of the 1979–2013 SST trend pattern. Two simulations are driven by 1981–2010 mean monthly sea ice concentrations, greenhouse gases, and ozone and run continuously for 50 years. The SST boundary condition in the first simulation is driven by a repeating annual cycle of the global monthly 1979–2013 SST trend at each grid point added to the monthly climatology. The SST boundary condition in the second simulation is the same as the first but with a uniform global SST 0.4 K subtracted, the latter being an idealization of the externally forced warming during this period occurring in coupled model simulations. The SST forcing used in this second experiment is thus an estimate of SST forcing that would have occurred without anthropogenic influences. Such an approach assumes that differences in the imposed basic state have little effect on the East African precipitation response.

The third simulation is a control run used to generate the mean monthly atmospheric response to climatological boundary conditions. The mean monthly atmospheric response is generated through averages of a 300-yr simulation driven by a repeating annual cycle of the 1981–2010 mean monthly SST, sea ice concentration, greenhouse gases, and ozone. The mean monthly atmospheric response is subtracted from the responses in the simulations described previously to identify the response to SST patterns.

c. *Coupled model simulations*

Two separate coupled model ensembles are utilized. The first ensemble comprises 40 members from the Community Earth System Model, version 1 (CESM1; Kay et al. 2015), drawn from the Large Ensemble Community Project (LENS). All CESM1 simulations are subject to the same radiative forcing: historical forcing from 1920 to 2005 and the representative concentration pathway 8.5 (RCP8.5) scenario after 2005. CESM1 uses CAM5 as its atmospheric component, and the coupled model is run at the same nominal spatial resolution as CAM5. The second ensemble comprises the first member of each of the 37 different CMIP5 models (Taylor et al. 2012) listed in Table 2. Each member of the transient coupled model runs of CMIP5 are subject to the same radiative forcing as the CESM1 simulations, historical forcing prior to 2005, and the RCP8.5 scenario thereafter. The CMIP5 models are nominally forced in the same manner, though there are differences arising from the fact that some models incorporate explicit chemistry, direct and indirect radiative effects of aerosol forcing, and various treatments of land surface changes. A comparison

TABLE 2. List of 37 CMIP5 models utilized. (Expansions of acronyms are available online at http://www.ametsoc.org/PubsAcronymList.)

Model	Institution
INM-CM4.0	Institute of Numerical Mathematics
BCC_CSM1.1	Beijing Climate Center
BCC_CSM1.1(m)	Beijing Climate Center
NorESM1-M	Norwegian Climate Centre
NorESM1-ME	Norwegian Climate Centre
MRI-CGCM3	Meteorological Research Institute
MPI-ESM-LR	Max Planck Institute for Meteorology
MPI-ESM-MR	Max Planck Institute for Meteorology
MPI-ESM-P	Max Planck Institute for Meteorology
MIROC5	Atmosphere and Ocean Research Institute (University of Tokyo), National Institute for Environmental Studies, and Japan Agency for Marine-Earth Science and Technology
MIROC-ESM	Atmosphere and Ocean Research Institute (University of Tokyo), National Institute for Environmental Studies, and Japan Agency for Marine-Earth Science and Technology
MIROC-ESM-CHEM	Atmosphere and Ocean Research Institute (University of Tokyo), National Institute for Environmental Studies, and Japan Agency for Marine-Earth Science and Technology
IPSL-CM5A-LR	L'Institut Pierre-Simon Laplace
IPSL-CM5A-MR	L'Institut Pierre-Simon Laplace
IPSL-CM5B-LR	L'Institut Pierre-Simon Laplace
HadGEM2-A	Met Office Hadley Centre
HadGEM2-CC	Met Office Hadley Centre
HadGEM2-ES	Met Office Hadley Centre
GISS-E2-H	NASA Goddard Institute for Space Studies
GISS-E2-R	NASA Goddard Institute for Space Studies
GFDL CM3	NOAA/Geophysical Fluid Dynamics Laboratory
GFDL-ESM2G	NOAA/Geophysical Fluid Dynamics Laboratory
GFDL-ESM2M	NOAA/Geophysical Fluid Dynamics Laboratory
FIO-ESM	First Institute of Oceanography, State Oceanic Administration
FGOALS-g2	LASG, Institute of Atmospheric Physics, Chinese Academy of Sciences; and CESS, Tsinghua University
FGOALS-s2	LASG, Institute of Atmospheric Physics, Chinese Academy of Sciences
CanESM2	Canadian Centre for Climate Modelling and Analysis
CSIRO Mk3.6.0	Commonwealth Scientific and Industrial Research Organisation in collaboration with the Queensland Climate Change Centre of Excellence
CNRM-CM5	Centre National de Recherches Météorologiques/Centre Européen de Recherche et de Formation Avancée en Calcul Scientifique
CMCC-CM	Centro Euro-Mediterraneo per I Cambiamenti Climatici
CMCC-CMS	Centro Euro-Mediterraneo per I Cambiamenti Climatici
CESM1(CAM5)	National Science Foundation, U.S. Department of Energy, and National Center for Atmospheric Research
CESM1(BGC)	National Science Foundation, U.S. Department of Energy, and National Center for Atmospheric Research
CCSM4	National Center for Atmospheric Research
BNU-ESM	College of Global Change and Earth System Science, Beijing Normal University
ACCESS1.0	Commonwealth Scientific and Industrial Research Organisation and Bureau of Meteorology
ACCESS1.3	Commonwealth Scientific and Industrial Research Organisation and Bureau of Meteorology

of the seasonal cycle of CESM1 and CMIP5 precipitation with observations indicates that the models capture the bimodality of East African precipitation but overestimate the magnitude of the October–December rains and underestimate the magnitude of the March–May rains (Fig. 2; see also Tierney et al. 2015). The externally forced signal of 1979–2013 East African rainfall trends is derived from the ensemble mean of the two coupled model ensembles, while the spread around those arises from unforced internal coupled ocean–atmospheric–land surface variability alone. In the case of the CMIP5 ensemble, the

interpretation of the spread about its ensemble mean is more complicated, owing to the fact that different models can have different sensitivity to external forcing.

3. Results

a. *Characterizing the March–May 1979–2013 East African precipitation trend*

An observed drying trend during 1979–2013 was widespread and spatially coherent over East Africa (Fig. 1b). At local scales, a linear fit to the 1979–2013 time series of rainfall reveals statistically significant drying (90% confidence level) across much of Ethiopia, southern Somalia, and small portions of Kenya and Tanzania. Interannual variability is nonetheless quite large at these local scales, and a linear drying trend is not detectable (at the 90% level) at many other grid points across the study domain. The magnitude of the 35-yr decline in March–May precipitation, averaged over the red box of Fig. 1b, is approximately 0.6 mm day, which is large from a historical perspective and corresponds to a two-standard-deviation departure of the statistics of all 35-yr trends computed from consecutive samples of data spanning 1901–2013 (Fig. 1c). Consistent with this, the time series of the average rainfall of East Africa (Fig. 3) describes a decline that is significant at the 95% level.

A central question of this study is the physical relationship between this recent decline in East African rainfall and climate drivers operating during the period. One characterization of the observed drying is that it has been atypical, for instance the unusual string of consecutive dry March–May seasons during 1997–2012, which might suggest effects of some sustained forcing (Fig. 3). Yet, the magnitude of the 35-yr drying trend itself appears not to have been unprecedented—a noteworthy feature of the historical time series is the occurrence of comparably strong drying trends at the beginning and end of the record (Fig. 3b). Certain aspects of climate forcing in recent decades have been unique, however, and would suggest the recent drying is not symptomatic of natural variability alone. Increasing external radiative forcing is the most obvious, a symptom of which has been an overall warming of the oceans. Figure 1a shows the linear trend in March–May SSTs during 1979–2013, which indicates a prevailing global ocean warming. Temperatures have not warmed in all basins, however, with an observed cooling trend over the central and eastern Pacific Ocean during 1979–2013.

It has already been demonstrated using atmospheric climate model simulations that recent East Africa drying has unlikely resulted from unforced internal atmospheric variability alone but is consistent with the region's sensitivity to SST variations occurring during the period (Lyon and DeWitt 2012; Liebmann et al. 2014). Here we present additional evidence for the presence of such an SST-forced signal using ensembles of AMIP simulations from two separate atmospheric models subjected to identical observed time-varying boundary conditions. The ensemble mean trend of both models reproduce key observed features of drying over East Africa during March–May 1979–2013 (Figs. 4a,c). The forced signal consists of a spatially coherent and widespread drying over all East Africa, the area-averaged magnitude of which is remarkably close to the estimated observed drying trend. Drying is reproduced in the vast majority of model realizations as indicated by the appreciable shift of the probability density functions (PDFs) of East African areally averaged trends toward negative values (Figs. 4b,d). The mean drying trend of the models corresponds to about 1.5–1.7 standardized departures relative to the internal atmospheric noise of 35-yr trends (Figs. 4b,d). The statistical distribution of simulated trends thus indicates that drying at least as severe as that which occurred during 1979–2013 had about 50% likelihood, given the actual forcing during this period. The probability is low (less than ~10%) that such multidecadal drying could have occurred because of random atmospheric noise alone since the standard deviation among the models' 35-yr rainfall trends, a symptom of unforced atmospheric variability, is appreciably less than the forced signal. The two ensembles of AMIP simulations thereby affirm arguments for the existence of a strong forced drying by SST over East Africa, as first presented in Lyon and DeWitt (2012).

By contrast, the coupled model simulations (CESM1 and CMIP5) indicate a much more modest ensemble mean signal of 35-yr rainfall trends resulting from external radiative forcing alone (Fig. 5), consistent with prior studies (e.g., Shongwe et al. 2011; Otieno and Anyah 2013; Kent et al. 2015; Tierney et al. 2015). For CESM1, externally forced drying is found over southern Ethiopia during 1979–2013, though little drying elsewhere over East Africa. The statistics of areally averaged East African precipitation trends computed for each model realization (see PDF in Fig. 5c) indicates a shift in probabilities toward drying, though of much more modest proportions than occurring in the AMIP simulations. The overall distribution function is found to be statistically different (at $p = 0.10$ using a Kolmogorov–Smirnov test) from the PDF of 35-yr rainfall trends simulated in CESM1 for the 1921–55 period before appreciable climate change forcing occurred. By contrast, no significant change in the spatial pattern or in the areally averaged statistics of 35-yr rainfall trends occurs in the CMIP5 ensemble

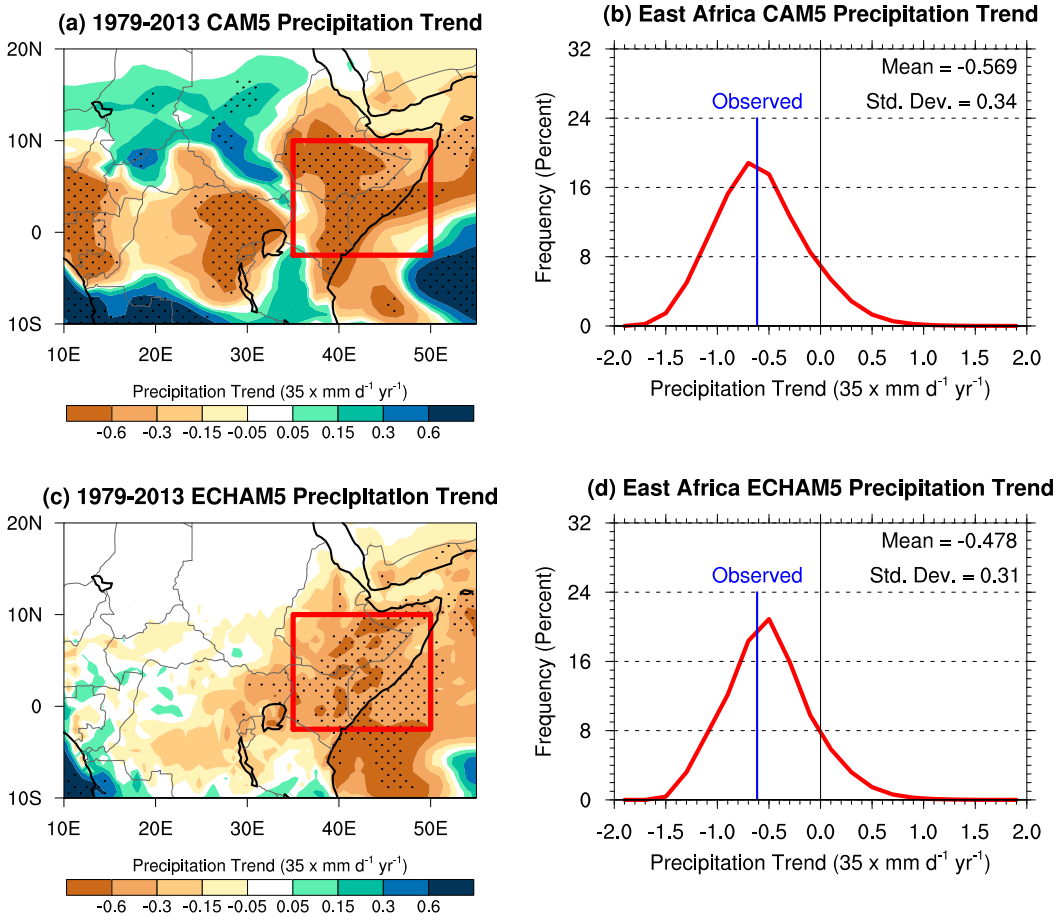

FIG. 4. March–May 1979–2013 trends of (a),(c) ensemble-average AMIP precipitation, where stippling denotes that 75% of the ensemble members have the same sign and (b),(d) areally averaged precipitation PDFs of East Africa constructed from AMIP ensemble members in (a),(b) CAM5 and (c),(d) ECHAM5.4.

(Figs. 5e,f). The PDF of all samples of CMIP5 rainfall trends indicates a maximum likelihood having no change, in contrast to a maximum likelihood of slight drying occurring in the CESM1 simulations and the much stronger drying occurring in historical AMIP simulations (cf. Fig. 4). Both coupled model ensembles agree in their suggestion, however, that a tail event having drying as strong as observed was more likely under the influence of external forcing during 1979–2013 compared to the earlier twentieth century. We will subsequently diagnose the global climate context for those extreme drying trend simulations.

The CESM1 and CMIP5 ensembles also indicate that the observed drying could have resulted from a very low-probability outcome of internal variability alone. The internal spread of 35-yr East African rainfall trends among the coupled model members is about 0.3 mm day^{-1}, similar in magnitude to that occurring in the AMIP ensemble. Thus, despite suggestions that recent external forcing may have increased in the likelihood of the observed East Africa drying (relative to 1921–55), the event was still a low-probability occurrence. Only in the AMIP ensemble is the likelihood for such a severe drying greatly increased, a consequence of the particular SST forcing operating during 1979–2013.

Revealed herein is an acute sensitivity of East African rainfall to the particular history of SSTs during 1979–2013 but a comparative insensitivity to the particular history of external radiative forcing alone. We note that the AMIP simulations are subjected to very similar external forcings to those driving the transient coupled model simulations; identical time series of external forcings are in fact used in CAM5 and CESM1. As such, differences between the observed SST trend (specified in AMIP) and SST trends in response to external forcing (in coupled models) must be a key factor explaining differences in East African rainfall responses among these models. Whereas CESM1 and CMIP5 ensemble mean SST trends describe a relatively uniform pattern of

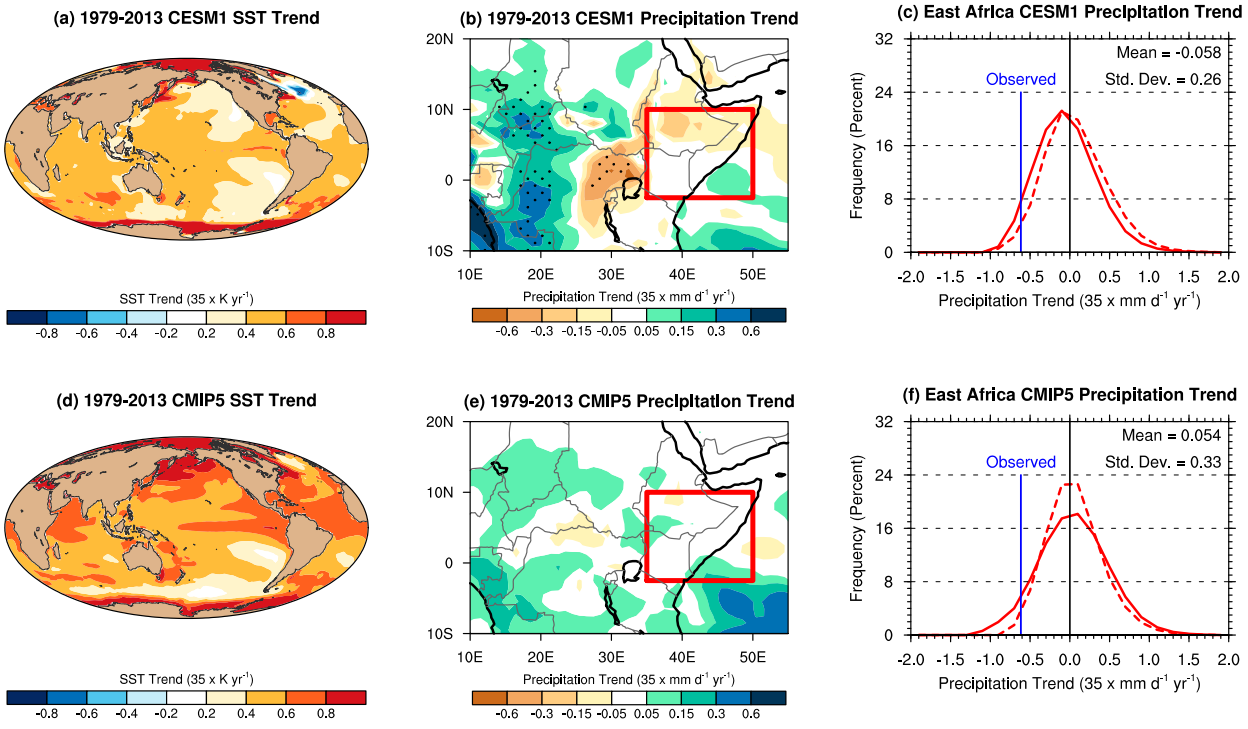

FIG. 5. March–May 1979–2013 trends of (a),(d) ensemble-average SST, (b),(e) ensemble-average precipitation, where stippling denotes that 75% of the ensemble members have the same sign, and (c),(f) areally averaged precipitation PDFs (solid line) of East Africa constructed from ensemble members in (a)–(c) CESM1 and (d)–(f) CMIP5. Precipitation PDFs of March–May 1921–55 East African trends constructed from ensemble members in CESM1 and CMIP5 are displayed as dashed lines. The p values testing the differences between the areally averaged East African 1979–2013 and 1921–55 PDFs are 0.56 for CMIP5 and 0.10 for CESM1 using a two-sample Kolmogorov–Smirnov test.

warming over all ocean basins (Figs. 5a,d), large spatial variations describe the observed trend pattern (cf. Fig. 1). The most prominent difference occurs over the tropical eastern Pacific Ocean where a large-scale cooling trend has occurred during 1979–2013 rather than the coupled model warming trend signal.

Our finding of major differences between the observed SST change since 1979 and those simulated in coupled models, together with indications that these have major consequences for regional climate, is not novel or surprising (see, e.g., Hoerling et al. 2006, 2010, 2016; Perlwitz et al. 2009). Nor does that fact alone reconcile existing theories on underlying causes for East Africa drying. A careful explanation of the particular observed SST history remains to be given, including clarifying its relation to climate change and identifying if some interplay between them exists as concerns East African rainfall sensitivity during 1979–2013. One aspect of the observed SST change believed to be key for East Africa drying as mentioned in the introduction is a strengthening of the contrast between SSTs of the western Pacific warm pool region and the central Pacific cold tongue. This strengthening is evident by comparing SST trends in two geographic regions used to define the WPG index, shown by the black boxes in Fig. 1a. The WPG gradient has increased by about 0.8°C during 1979–2013. By contrast, the ensemble mean SST response to radiative forcing in both coupled model ensembles indicates a near-uniform warming of the tropical oceans, with comparatively little change in the WPG (Figs. 5a,d).

A plausible interpretation of the particular observed history of SST change since 1979 is therefore that it commingles a pattern of overall ocean warming due to radiative forcing with a multidecadal variation of mostly natural origins. Analogous to the method of event attribution used in Lott et al. (2013), estimates of this internal component can be derived by removing the externally forced signal from the 1979–2013 observed trend. Figure 6 shows these estimates, based on removing the ensemble mean 1979–2013 trends derived from the CESM1 and CMIP5 coupled model suites. The residual shows a familiar pattern that includes equatorial central Pacific coolness enveloped by a horseshoe-like pattern of average and above-average SST, having maximum amplitudes over the North and South Pacific basins. They both resemble the cold tropical phase of the

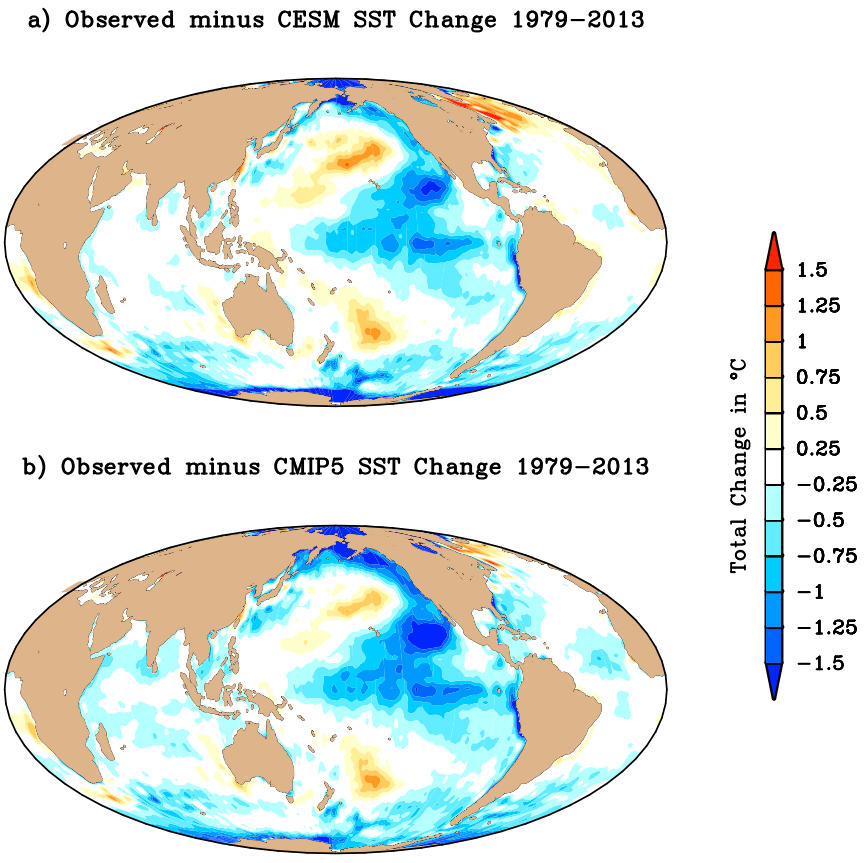

FIG. 6. Observed March–May 1979–2013 SST trend minus the (a) ensemble-average CESM SST trend (Fig. 4a) and (b) ensemble-average CMIP5 SST trend (Fig. 4d).

ENSO-like Pacific decadal variation (Zhang et al. 1997; Mantua et al. 1997), and furthermore these residuals also resemble the observed difference between time mean SSTs for 1943–76 minus 1925–42 (see Fig. 15a of Zhang et al. 1997). A linear combination of an overall warming in global SSTs due to climate change with a known pattern of low-frequency ENSO-like variability thus offers a reasonable physical explanation for the 1979–2013 history of observed SST change. The latter source of variability has mostly been responsible for altering spatial gradients in SSTs, especially the zonal contrast between the warm pool and cold tongue regions. Evidence will be subsequently provided indicating that such internal fluctuation in tropical Pacific SSTs, as measured by intensification of the WPG index, was an extreme expression of natural decadal variability.

b. *Anthropogenic influences on decadal-to-multidecadal East African precipitation trends*

We next estimate anthropogenic influences on observed East Africa drying since 1979 using the CESM1 and CMIP5 coupled climate model ensembles that are assumed to adequately represent the physics of East African climate (see section 4 for further discussion). Our initial finding is that the unconditional probability of East African rainfall decline during 1979–2013 was unaffected by climate change in the CMIP5 ensemble but affected by climate change over southern Ethiopia in the CESM1 (see Fig. 5). In this section we explore the conditional probability, recognizing the presence of a cold phase ENSO-like Pacific decadal oscillation during this recent period. Our approach involves distinguishing effects of such internal Pacific decadal SST variations on East African rainfall when they arise in the current warmed climate versus in an earlier climate antecedent to appreciable anthropogenic warming. Since there are insufficient historical analogs of such multidecadal variations from which to draw empirical estimates, we utilize our transient simulations of the all-forcings historical CESM1 and CMIP5 models to construct composites. The approach here is analogous to that used in Christidis and Stott (2014), who used all forcing (ALL) and natural forcing (NAT) coupled model experiments to examine how climate change alters probabilities of extreme seasonal rainfall over the United

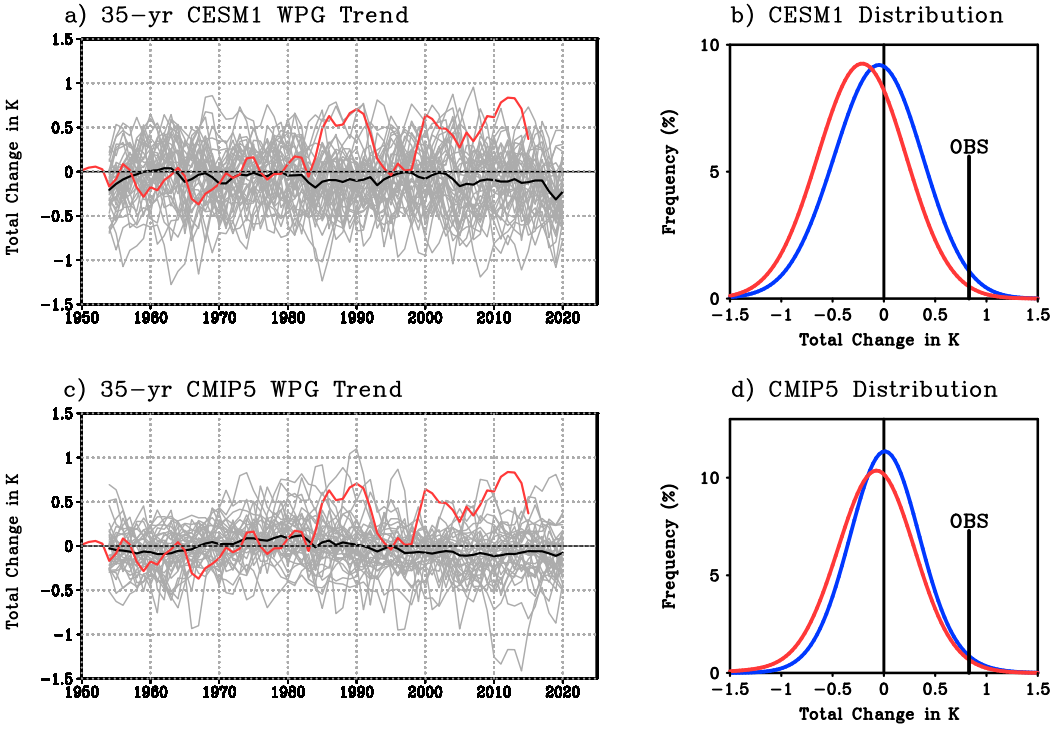

FIG. 7. The 35-yr end-point trends of the WPG in observation (red line), ensemble average (black line), and ensemble members (gray lines) in (a) CESM1 and (c) CMIP5. PDFs of 35-yr end-point trends of the WPG for end points after 2000 (red line) and end points prior to 1990 (blue line) for (b) CESM1 and (d) CMIP5.

Kingdom, conditioned on a particular phase of atmospheric circulation. It differs from the method of Lott et al. (2013), who used atmospheric model simulations subjected to actual SSTs and counterfactual SSTs of a "world that might have been" in order to determine human contributions to 2011 extreme East African drought. An implementation of the Lott et al. (2013) approach would involve comparing statistics of East African rainfall in atmospheric climate simulations subjected to the SST patterns of Fig. 1a versus the SST patterns in which anthropogenic forcing is removed. The discussion section will address the robustness of our findings across various methods and contrast results from coupled model methods used herein to those from techniques based on atmospheric model methods.

Using the WPG index to infer ENSO-like multidecadal variability, we construct time series of moving 35-yr trends in the WPG for both observations (Fig. 7, red curve) and for each historical run of the coupled models (Fig. 7, gray curves). The common period for the SST time series is 1920–2015. Observed values of March–May 35-yr WPG trends are generally small in the first half of the record compared to the last half. Further, all WPG trends have been positive signed for 35-yr periods beginning in the 1951–85 period and continuing to present, indicating strengthened zonal contrasts of SSTs between the western and central equatorial Pacific (see also Hoell et al. 2013). Individual model samples of simulated 35-yr WPG trends exhibit great variability from the beginning to the end of the record and also show considerable differences from run to run (Figs. 7a,c, gray lines). In this sense, the observed behavior of WPG trends during 1920–2015 is broadly consistent with the statistics of two coupled model ensembles and falls within the spread of each model suite. However, the forced signal of change, as estimated from the ensemble average of the model data (black curves), is toward more negative (weakened) WPG in contrast to a trend toward more positive (strengthened) WPG in observations. This tendency, associated with an El Niño–like pattern of SST response to external radiative forcing (see Fig. 5), is nonetheless small when compared to the spread of 35-yr trend statistics. Indeed, there are positive WPG trends near the magnitude observed in a few model samples during the recent decades of strong global warming. As such, it cannot be discounted that the observed tendency for predominately positive WPG trend occurrences in the last half-century of the observational record is indicative of mostly natural variability, the magnitude of which could be masking the climate change signal toward slightly more negative WPG index values.

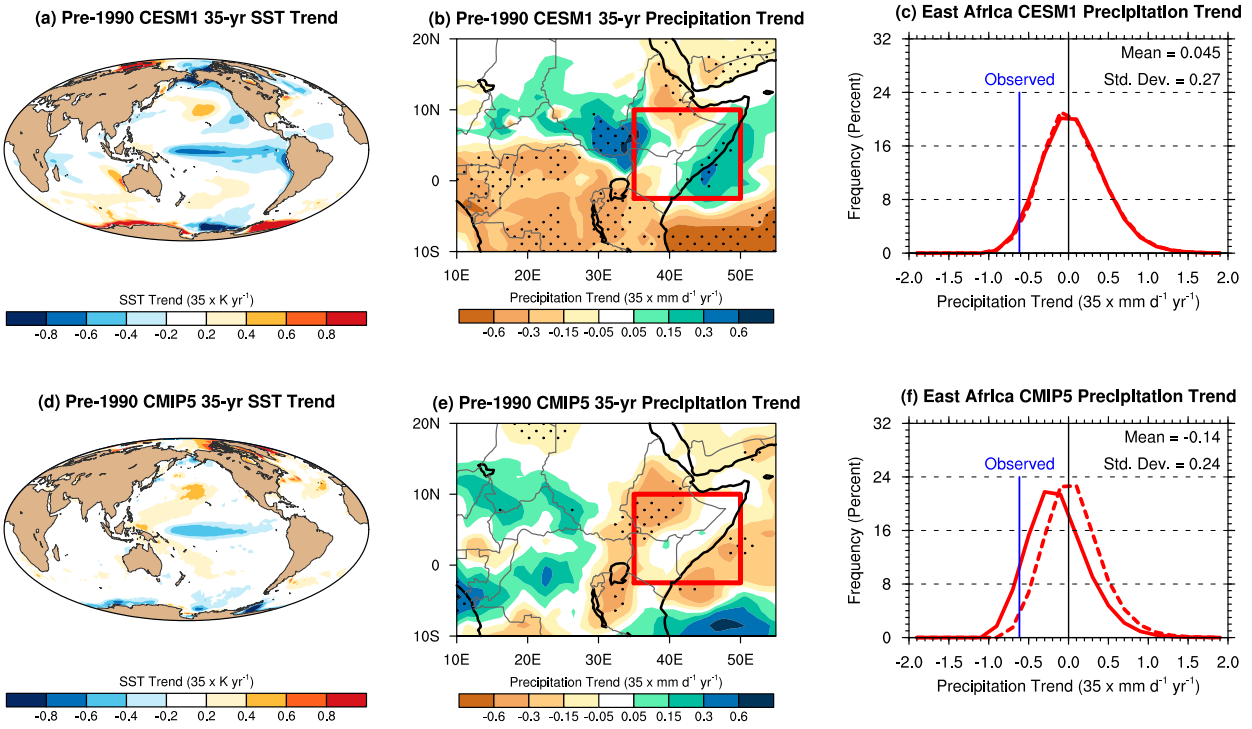

FIG. 8. The 35-yr March–May trends of (a),(d) ensemble-average SST, (b),(e) ensemble-average precipitation, where stippling denotes that 75% of the ensemble members have the same sign, and (c),(f) areally averaged precipitation PDFs of East Africa (solid line) constructed from ensemble members in (a)–(c) CESM1 and (d)–(f) CMIP5 for 35-yr trends of the WPG exceeding 0.6 K with an end-point year before 1990. Precipitation PDFs of March–May 1921–55 East African trends constructed from all ensemble members of CESM1 and CMIP5 are displayed as dashed lines. The p values testing the differences between the PDFs of areally averaged East African pre-1990 trends during a strong WPG and 1921–55 trends are 0.01 for CMIP5 and 0.73 for CESM1 using a two-sample Kolmogorov–Smirnov test.

It is noteworthy that the magnitude of observed WPG strengthening during 1979–2013 appears to be an extreme event when measured against all samples of 35-yr trends in both CESM1 and CMIP5 distributions (Fig. 7b,d). Both models have samples of comparably strong gradient strengthening events, but these comprise less than 5% of all samples. There is little evidence from the time series that occurrences of such extreme events either increase or decrease during the early twenty-first century compared to the mid-twentieth century, despite the overall climate change signal to a slightly weaker contrast in SSTs between the warm pool and cold tongue regions. It is thus likely that natural multidecadal SST variability of an extreme magnitude prevailed in recent decades and was mainly responsible for intensifying the WPG, despite an overall slight weakening of the WPG by external forcing.

Using the positive index values of the WPG as proxies for ENSO-like Pacific decadal cold periods, composites of associated East African rainfall are constructed for mid-twentieth-century and near-current climate conditions. A threshold value for a 35-yr trend in the WPG index of +0.6 is used, which represents a compromise between selecting the extreme observed index value during 1979–2013 as threshold (+0.8), while permitting a meaningful sample size. Under this construct 27 cases are available for CESM1 and 26 for CMIP5. Figure 8 shows the composite for the earlier record (which includes all 35-yr periods beginning in 1920 and ending in 1989), based on CESM1 (Fig. 8a–c) and CMIP5 (Fig. 8d–f) simulations. The SST composite trend patterns associated with WPG strengthening resembles well-known structures of Pacific decadal variability (Fig. 8a,d). Strong coolness in the central Pacific is flanked in the western Pacific and the extratropical Pacific by warm SST anomalies. A mostly weak and spatially incoherent pattern of rainfall trends is associated with this composite of cold ENSO-like decadal states (Fig. 8b,e). The PDF of area-averaged rainfall trends for CESM1 indicates little preference for either dry or wet conditions, while that derived from CMIP5 samples indicates a shift toward increased dry-trend probabilities. Only for CMIP5 is the overall distribution function of conditional probabilities associated with strong WPG periods significantly different from the unconditional probabilities (at $p = 0.10$ using a Kolmogorov–Smirnov test), the latter PDF derived from 35-yr rainfall trends for all samples during the

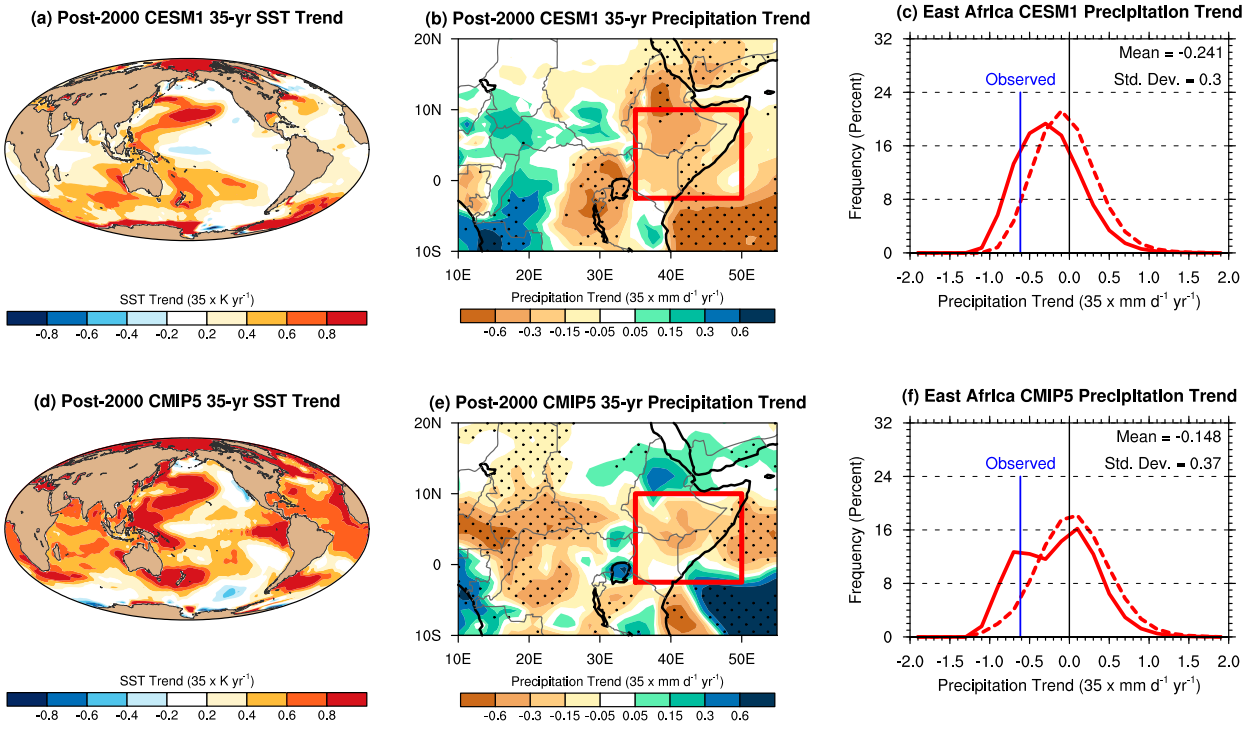

FIG. 9. The 35-yr March–May trends of (a),(d) ensemble-average SST, (b),(e) ensemble-average precipitation, where stippling denotes that 75% of the ensemble members have the same sign, and (c),(f) areally averaged precipitation PDFs of East Africa (solid line) constructed from ensemble members in (a)–(c) CESM1 and (d)–(f) CMIP5 for 35-yr trends of the WPG exceeding 0.6 K with an end-point year after 2000. Precipitation PDFs of March–May 1979–2013 East African trends constructed from all ensemble members of CESM1 and CMIP5 are displayed as dashed lines. The p values testing the differences between the PDFs of areally averaged East African post-2000 trends during a strong WPG and 1979–2013 trends are 0.31 for CMIP5 and 0.04 for CESM1 using a two-sample Kolmogorov–Smirnov test.

1921–55 period. These coupled model results for a period before appreciable global warming are quite different from the AMIP results for 1979–2013, which reveal a much stronger 35-yr forced trend over East Africa associated with an occurrence of recent WPG strengthening. Indicated hereby is that a cold phase of the ENSO-like multidecadal oscillation acting alone is unlikely a principal cause for the recent East Africa drying. Further, these results also indicate that while the East Africa drying was indeed strongly forced (as per AMIP), the forcing is unlikely attributable to natural variability alone.

Figure 9 repeats the analysis, but for composites based on the recent record (which includes all 35-yr periods beginning in 1966 and ending in 2020). Because of an ensemble mean trend toward a negative WPG index, there are appreciably fewer model samples of WPG 35-yr trend events exceeding +0.6°C, with only 15 cases available for CESM1 and 7 cases for CMIP5 simulations. Further, most of the CMIP5 samples are drawn from a single simulation, the CMCC-CMS model, since several trends with different end points meet the WPG criteria and are each included in the sample. The composite SST trend patterns are structurally similar to those derived from the earlier epoch, but with less cooling in the cold tongue, greater warming in the warm pool, and a better-defined horseshoe of warm SSTs that encircle the equatorial central Pacific minimum. Many of these SST features align better with the actual observed SST trend pattern of 1979–2013 (cf. Fig. 1), except that the observed contains an even stronger central and eastern Pacific cooling trend than in either of these composites. Composites of the models' East African rainfall trends indicate a more spatially coherent pattern having widespread drying. The CESM1 composite is particularly dry, with an area-averaged mean trend of $-0.24\,\mathrm{mm\,day^{-1}}$. The CESM1 PDF indicates a clear shift toward dry trend likelihoods, with 12 of the 15 samples yielding drying, and a maximum likelihood as estimated from the mode of the distribution being about $-0.3\,\mathrm{mm\,day^{-1}}$, assuming the coupled runs fully sample the possible climate conditions. This compares with the observed drying trend magnitude of about $-0.6\,\mathrm{mm\,day^{-1}}$. Importantly, the CESM1 result reveals a significant shift in the likelihood of East Africa drying during enhanced WPG periods in the current relative to earlier climate state. We also note that the results of the Kolmogorov–Smirnov test indicate

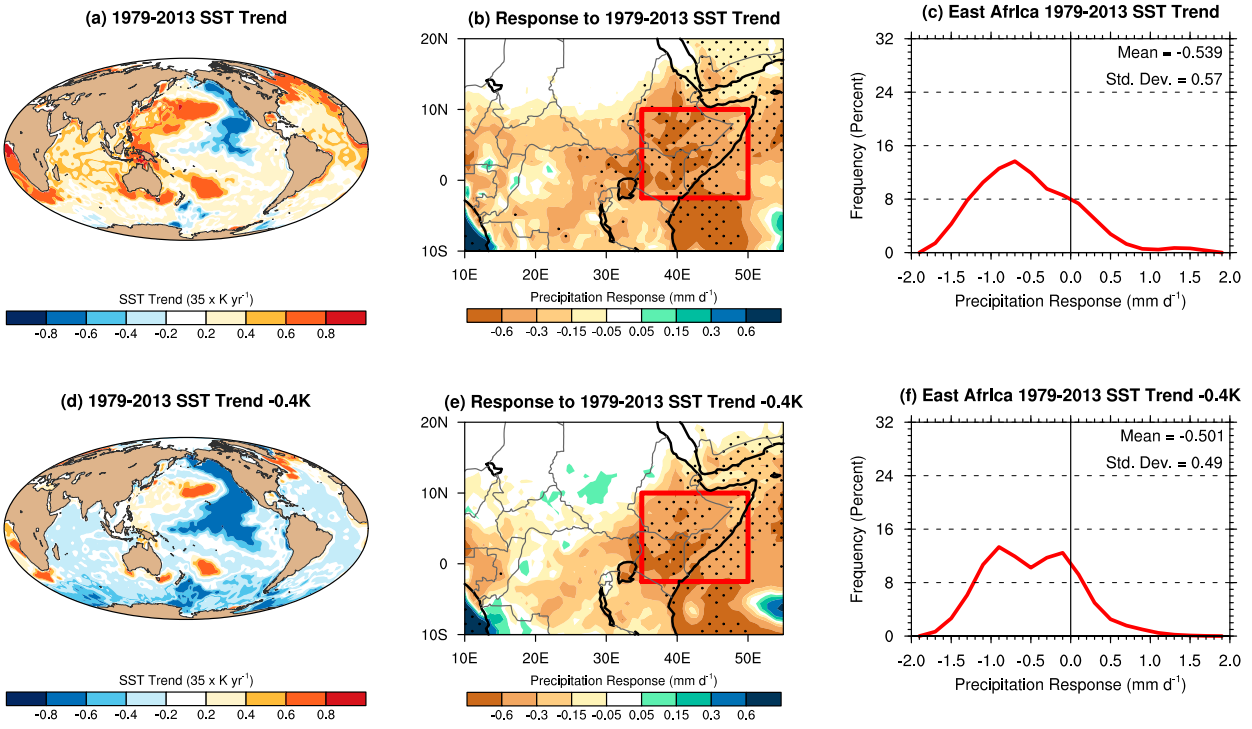

FIG. 10. Precipitation response in ECHAM5.4 to the (a) March–May 1979–2013 SST trend pattern displayed (b) spatially for the ensemble average, where stippling denotes that 75% of the ensemble members have the same sign, and (c) areally averaged precipitation PDFs of East Africa constructed from the ensemble members. Precipitation response in ECHAM5.4 to the (d) March–May 1979–2013 SST trend pattern with uniform 0.4 K subtracted displayed (e) spatially for the ensemble average, where stippling denotes that 75% of the ensemble members have the same sign, and (f) areally averaged precipitation PDFs of East Africa constructed from the ensemble members.

that the conditional PDF of 35-yr trends for the current period is highly significantly different from the unconditional PDF (at $p = 0.04$). The CMIP5 results are less definitive in this regard, owing in part to the smaller sample sizes, which make it particularly difficult to estimate the recent PDF reliably (and in part owing to the small sample size of only seven cases, the Kolmogorov–Smirnov test does not indicate significant differences at $p < 0.10$).

Overall, the results from the CESM coupled climate simulations are suggestive that human-induced change altered the tropical-wide teleconnections linking East African March–May rainfall with cold states of ENSO-like Pacific decadal variability. That connection has either emerged or become more effective in recent decades when such fluctuations are arising in concert with appreciable global warming. An important interplay between a human-induced warming of the oceans and a naturally occurring internal oceanic fluctuation is therefore potentially key, the coaction of which offers a plausible physical explanation for the observed East Africa drying. The paradigm is one in which both natural variability and climate change were necessary insofar as a forced drying may not have occurred if either factor operated alone. It is important to note, however, that the same inference cannot be drawn from CMIP5. Owing in part to sampling issues and perhaps also to structural uncertainty among different models, our parallel analysis of CMIP5 multimodel ensembles does not yield the same behavior as found in the CESM1 large ensemble.

In light of the conflicting results generated from the CESM1 and CMIP5 experiments, we use a different methodology to further test the sensitivity of East Africa drying to the cool phase of natural Pacific decadal variability in the presence of an externally forced warming of the western Pacific. We perform atmospheric model experiments using ECHAM5.4 in the spirit of the method used in Lott et al. (2013), in which we test the East African precipitation responses to the observed 1979–2013 SST trend and separately to an estimate of the 1979–2013 trend in a world in which climate change did not occur (Fig. 10). For the latter, we simply remove a global uniform SST warming from each oceanic grid point in order to derive a so-called counterfactual pattern of SSTs. We subtract 0.4 K from the observed 1979–2013 SST trend, which is an idealization

of the externally forced warming during this period in the coupled climate models (see Fig. 5). We note that the resulting counterfactual pattern of SST forcing, a proxy for the natural component of SST trend during 1979–2013, is quite similar to the residual SST patterns of Fig. 6. It also bears resemblance to the SST composites of CESM1 and CMIP5 for expressions of 35-yr WPG strengthening trends that occurred during the earlier twentieth century of the model simulations. (cf. Fig. 10d and Fig. 8). There is appreciably greater central Pacific cooling in this counterfactual, however. Likewise, the observed central Pacific cooling trend during 1979–2013 is considerably stronger than that occurring in the coupled model composites of 35-yr WPG strengthening trends that occurred during the early twenty-first century.

Strong amplitude and spatially coherent East African dryness occurs in response to the observed 1979–2013 SST trend pattern, similar to features of the East Africa drying trend occurring both in observations and AMIP simulations (cf. Figs. 10b,c and Fig. 3). A strong shift in the regional precipitation distribution to drought is evident, and the vast majority of the ensemble members simulate dryness. Virtually identical East African dryness occurs in response to the counterfactual SST forcing (Figs. 10e,f).[1] To the extent that this is a realistic depiction of the natural component of SST forcing during 1979–2013, these atmospheric model simulations suggest that global warming did not appreciably alter East African rainfall responses. The strong dry response to estimates of the natural pattern of SST change implies anthropogenic influences need not be invoked to explain the severity of observed drying, outwardly consistent with a weak East Africa drying only found in the CESM1 and CMIP5 unconditional simulations for 1979–2013 (see Fig. 5). Yet, the results of these idealized atmospheric model simulations are inconsistent with other CESM1 diagnostics that reveal appreciable East Africa drying when conditioned on occurrences of cool phases of ENSO-like decadal variability during 1979–2013 (see Fig. 9). It is unclear whether these two different perspectives are an indication of sensitivity to methodology involving coupled versus uncoupled model approaches, an expression of structural uncertainty owing to particular sensitivities of different models (regardless of coupling), an indication of sensitivity to the particular SST forcing that is used (which are not identical in the AMIP and CMIP approaches), or other factors. Further research is required to address these open questions.

[1] The experiments described in Fig. 10 still include anthropogenic forcing of the atmosphere, even though the SSTs have been adjusted to an estimated ''natural'' counterfactual state. Another counterfactual simulation that adjusts SST, sea ice, and the atmospheric trace gases (not shown) confirms the result of Fig. 10e. Those comprised a 10-member ECHAM5 AMIP suite in which the observed SST variations since 1979 were detrended by removing the observed 1880–2010 linear trend and also by setting greenhouse gas and ozone concentrations to their estimated 1880s values. The runs ended in 2012 and did not span the entire period under study herein. For 1979–2012, East African rainfall change in the realistic versus counterfactual AMIP runs exhibited near-identical drying.

4. Summary and discussion

Our study sought to reconcile two theories for the severe decline in March–May East African rains that occurred during 1979–2013, one conjecturing a mostly natural cause and the other a mostly human-induced cause. Our approach involved diagnosing the region's sensitivity to patterns of SST forcing using atmospheric models driven by observed SST variability, atmospheric models driven by idealizations of the observed SST trend pattern during 1979–2013, and coupled climate system models driven by historical radiative forcing in which SSTs freely evolve. We capitalized on evidence that atmospheric models driven by the actual time-varying boundary conditions reproduce the observed pattern of East Africa drying. We thus tested the two causality arguments by focusing on physical explanations for the natural and anthropogenic contributions to the observed SST trends and by identifying East African rainfall sensitivity to each forcing individually and combined. We did not explicitly explore other possible factors, such as effects of Arctic sea ice changes or sensitivity to direct radiative forcing including anthropogenic aerosols. Comparisons with idealized forcing experiments do, however, affirm a leading effect of SST driving.

Double-edged results were found insofar as evidence supporting both theories emerged. Concerning tests of an argument for mostly natural causes of the observed East Africa drying, we confirmed the existence for a strong internal multidecadal SST variation during this period describing the tropical Pacific cold phase of ENSO-like variability. We explored East African rainfall sensitivity to such forcing by first sampling CMIP5 simulated 35-yr tropical Pacific SST trend patterns resembling the observed 1979–2013 trend. A large ensemble of historical simulations was analyzed in which one run from each of 37 different coupled models was used in which equal weights were assigned to each simulation. Frequency distributions of East African rainfall were diagnosed, though recognizing that statistics of those PDFs included structural uncertainty among models in their responses to natural and anthropogenic forcing in addition to capturing common signals of such forcing effects. Samples of runs having

35-yr SST trends resembling a tropical Pacific cold phase of ENSO-like variability were extracted from the early- to mid-twentieth-century simulations. These revealed East African rainfall trends having only modest drying, with neither the intensity nor spatial scale of the recent observed drying trend. Samples of runs extracted from the early twenty-first-century simulations indicated similarly weak East Africa drying trends of weak magnitude. The East African rainfall sensitivity in CMIP5 was thus not materially different when the ENSO-like decadal SST mode was juxtaposed with human-induced global warming. Climate change forcing was also found to be ineffective when acting alone outside of southern Ethiopia (i.e., unconditioned upon the state of background internal variability), as demonstrated by the absence of appreciable rainfall change in the ensemble mean of the 1979–2013 transient runs of the CMIP5 ensemble. Overall, our analysis of CMIP5 data indicated only a weak drying sensitivity of East African rainfall to SST driving of the type operating in 1979–2013, with little indication for an appreciable effect of human-induced climate change.

Yet, a conflicting narrative of the underlying cause for recent East Africa drying emerges when using a differently constructed large ensemble dataset. A set of historical simulations was derived from a particular single model (CESM1) that provided 40 different re-enactments and from which a more physically realistic probability distribution of event likelihoods could be diagnosed. A limiting aspect in interpreting these distributions is that they may speak to a unique CESM1 behavior that does not necessarily pertain to a wider class of coupled models. Our study of those runs indicated an interplay between internal decadal SST variability and human-induced climate change that greatly increased the likelihood for strong East Africa drying during 1979–2013. First, we found no appreciable sensitivity of East African rainfall to cold phases of the ENSO-like decadal mode occurring in the early-to-mid-twentieth century, suggesting that natural decadal variability alone would not have explained recent East Africa drying. Second, a significant drying occurred in association with samples of such decadal variations that were drawn from the early twenty-first-century CESM1 simulations. Indeed, the odds of a drying trend equal to or greater than the observed drying during 1979–2013 trend increased tenfold when diagnosed in this conditional context. By contrast, 1979–2013 East African rainfall trends in the CESM1 ensemble unconditioned on the state of background internal ocean variability outside of southern Ethiopia were negligible, consistent with the CMIP5 results. Our analysis of CESM1 thus uncovered a strong mediating effect and an important interplay between human-induced ocean variations and a natural decadal cycle of ocean variation. It supports an argument that the strong East Africa drying during 1979–2013 seen in observations, and also simulated in the fully forced AMIP simulations for 1979–2013, may be symptomatic of a sensitivity to the joint occurrences of natural and human-induced variability in the global oceans.

Independent tests, using an atmospheric modeling approach, to disentangle natural versus anthropogenic factors provided compelling evidence for strong East African rainfall sensitivity to the natural component of SST-driving during 1979–2013. We forced a particular atmospheric model (ECHAM5.4) with a residual pattern of 1979–2013 SST trends in which an estimated human-induced SST change pattern indicated by the coupled model simulations was removed from the observed trend. This so-called counterfactual experiment produced a pattern and intensity of East African dryness that closely resembled the observed East African rainfall trends, that replicated the model response to the total SST trend pattern, and that also reproduced the drying occurring in atmospheric models driven by the actual time-varying boundary conditions. Those results were replicated in another set of atmospheric experiments that used a different treatment of the counterfactual SSTs and related anthropogenic forcings. In contrast, forcing the atmospheric model with just the estimated pattern of human-induced SST change, estimated as a globally uniform SST increase of 0.4 K, yielded no appreciable rainfall response over East Africa, akin to the lack of sensitivity in the ensemble average of CMIP models for 1979–2013.

Our analysis methods, datasets, and basic understanding are insufficient at this time to embrace with high confidence one line of evidence and reject the other regarding underlying causes for East Africa drying. All the coupled models have limitations in that the statistical sample of 35-yr trends in the western Pacific SST gradient having magnitudes equal to 1979–2013 trend are small. As a result, we were compelled to form composites using a somewhat lower threshold value of the WPG than occurred. This was especially true for the CMIP5 data, for which only a single model run of the 37 separate models contributed to our composite of early twenty-first-century analogs limiting any inferences that could be drawn from that very small sample. Indeed, our time series analysis of moving 35-yr trends in the WPG since 1920 indicated that the observed 1979–2013 central Pacific cooling was likely an expression of extreme decadal variability. Biases in SST variability within coupled models undoubtedly affect such appraisals, especially given a generally underestimated amplitude of tropical SST variability

on decadal–centennial time scales (e.g., Newman et al. 2016; Ault et al. 2013; Laepple and Huybers 2014). We also relied on a simple index of tropical Pacific SST variability from which to identify overall patterns of SST changes analogous to observations during 1979–2013. It is possible that other natural components of SST variability, not linearly related to a strengthened WPG, may have contributed to the 1979–2013 East Africa drying. However, we would note that atmospheric model simulations forced only by Pacific SSTs conducted as part of this study (not shown) reproduce the Lyon and DeWitt (2012) finding that the Pacific SST changes during 1979–2013 mainly drove the East Africa drying occurring in the fully forced atmospheric model simulations.

Other confounding issues, which we are unable to quantify in this study, include biases in CMIP5 and CESM1 SST responses to external forcings themselves. The ensemble means of those systems yield a mostly uniform pattern of tropical ocean warming during 1979–2013. The possibility that coupled climate models are too sensitive to greenhouse forcing in the tropical Pacific has been noted (e.g., Yeh et al. 2012), and it cannot be discounted that the true externally forced signal of SST change since 1979 has considerable spatial inhomogeneities. For example, interdecadal variability in anthropogenic aerosols is likely important, and there is considerable model uncertainty both in representing the aerosol forcing itself and in the associated climate sensitivity (e.g., Wilcox et al. 2013). It is not currently known, however, how these various biases in coupled climate models or in their forcing might yield a spatially varying articulation and especially whether they might project onto an increased WPG pattern as occurred during 1979–2013.

In summary, it is our interpretation that the WPG intensification during the 35-yr period of 1979–2013, to which East Africa drying was judged to be particularly sensitive based on our various AMIP experiments, was a historic event of the century-long record. Furthermore, it is our interpretation from current knowledge that the magnitude of this oceanic extreme event resulted from natural variability primarily. Various lines of evidence indicate that this SST pattern, immersed within an overall warmer climate, forced much of the East Africa drying since 1979 of a magnitude that could not readily have occurred without SST forcing. We believe that climate change forcing alone could not have generated such a forced drying. We are intrigued by the CESM1 large ensemble result that indicates a combination of such natural variability with climate change could have dramatically increased the odds of a secular drying over East Africa during 1979–2013. The possibility that regional climate may be sensitive to synergies between modes of natural variability and climate change has not been extensively explored (see, e.g., Christidis and Stott 2014; Wang et al. 2015), and the CESM1 results are quite dramatic in their suggestion for strong conditionality of the climate change impacts. Additional studies using large ensembles from other modeling centers will therefore be useful to test the results presented herein, an example being the recently generated 100-member Second Generation Canadian Earth System Model (CanESM2) ensemble spanning 1950–2015 (Sigmond and Fyfe 2016). It is also important for future work on East African climate trends to further explore how anthropogenic influences may modify the WPG, including a better understanding of the ocean dynamics and physical processes underpinning the unusual 1979–2013 central Pacific cooling. Better understanding the interplay of natural variability and climate change is therefore necessary to inform adaptation and mitigation strategies to alleviate the catastrophic effects of East African drought (Hillbruner and Moloney 2012) and better anticipate future conditions.

Acknowledgments. The authors thank Chris Funk for comments offered on earlier versions of this manuscript. The authors also thank three anonymous reviewers for thoughtful and constructive comments, Daithi Stone and Michael Wehner of the Computational Research Division at the Lawrence Berkeley National Laboratory for access to CAM5 simulations, and Dave Allured for completing the ECHAM5.4 simulations. The authors are grateful for support from the Famine Early Warning Systems Network.

REFERENCES

Adler, R. F., and Coauthors, 2003: The Version-2 Global Precipitation Climatology Project (GPCP) monthly precipitation analysis (1979–present). *J. Hydrometeor.*, **4**, 1147–1167, doi:10.1175/1525-7541(2003)004<1147:TVGPCP>2.0.CO;2.

Ault, T. R., C. Deser, M. Newman, and J. Emile-Geay, 2013: Characterizing decadal to centennial variability in the equatorial Pacific during the last millennium. *Geophys. Res. Lett.*, **40**, 3450–3456, doi:10.1002/grl.50647.

Becker, A., P. Finger, A. Meyer-Christoffer, B. Rudolf, K. Schamm, U. Schneider, and M. Ziese, 2013: A description of the global land-surface precipitation data products of the Global Precipitation Climatology Centre with sample applications including centennial (trend) analysis from 1901–present. *Earth Syst. Sci. Data*, **5**, 71–99, doi:10.5194/essd-5-71-2013.

Christidis, N., and P. A. Stott, 2014: Change in the odds of warm years and seasons due to anthropogenic influence on the climate. *J. Climate*, **27**, 2607–2621, doi:10.1175/JCLI-D-13-00563.1.

Cionni, I., and Coauthors, 2011: Ozone database in support of CMIP5 simulations: Results and corresponding radiative forcing. *Atmos. Chem. Phys.*, **11**, 11 267–11 292, doi:10.5194/acpd-11-10875-2011.

Compo, G. P., and P. D. Sardeshmukh, 2010: Removing ENSO-related variations from the climate record. *J. Climate*, **23**, 1957–1978, doi:10.1175/2009JCLI2735.1.

Conley, A. J., and Coauthors, 2012: Description of the NCAR Community Atmosphere Model (CAM 5.0). NCAR Tech. Note NCAR/TN-486+STR, 289 pp. [Available online at http://www.cesm.ucar.edu/models/cesm1.0/cam/docs/description/cam5_desc.pdf.]

Funk, C., and A. Hoell, 2015: The leading mode of observed and CMIP5 ENSO-residual sea surface temperatures and associated changes in Indo-Pacific climate. *J. Climate*, **28**, 4309–4329, doi:10.1175/JCLI-D-14-00334.1.

——, M. D. Dettinger, J. C. Michaelsen, J. P. Verdin, M. E. Brown, M. Barlow, and A. Hoell, 2008: Warming of the Indian Ocean threatens eastern and southern African food security but could be mitigated by agricultural development. *Proc. Natl. Acad. Sci. USA*, **105**, 11 081–11 086, doi:10.1073/pnas.0708196105.

——, S. E. Nicholson, M. Landsfeld, D. Klotter, P. Peterson, and L. Harrison, 2015a: The centennial trends Greater Horn of Africa precipitation dataset. *Sci. Data*, **2**, 150050, doi:10.1038/sdata.2015.50.

——, and Coauthors, 2015b: The climate hazards infrared precipitation with stations—A new environmental record for monitoring extremes. *Sci. Data*, **2**, 150066, doi:10.1038/sdata.2015.66.

Gates, W. L., 1992: AMIP: The Atmospheric Model Intercomparison Project. *Bull. Amer. Meteor. Soc.*, **73**, 1962–1970, doi:10.1175/1520-0477(1992)073<1962:ATAMIP>2.0.CO;2.

Guemas, V., S. Corti, J. García-Serrano, F. J. Doblas-Reyes, M. Balmaseda, and L. Magnusson, 2013: The Indian Ocean: The region of highest skill worldwide in decadal climate prediction. *J. Climate*, **26**, 726–739, doi:10.1175/JCLI-D-12-00049.1.

Hillbruner, C., and G. Moloney, 2012: When early warning is not enough—Lessons learned from the 2011 Somalia Famine. *Global Food Secur.*, **1**, 20–28, doi:10.1016/j.gfs.2012.08.001.

Hoell, A., and C. Funk, 2013: The ENSO-related west Pacific sea surface temperature gradient. *J. Climate*, **26**, 9545–9562, doi:10.1175/JCLI-D-12-00344.1.

——, and ——, 2014: Indo-Pacific sea surface temperature influences on failed consecutive rainy seasons over eastern Africa. *Climate Dyn.*, **43**, 1645–1660, doi:10.1007/s00382-013-1991-6.

Hoerling, M., J. Hurrell, J. Eischeid, and A. Phillips, 2006: Detection and attribution of twentieth-century northern and southern African rainfall change. *J. Climate*, **19**, 3989–4008, doi:10.1175/JCLI3842.1.

——, J. Eischeid, and J. Perlwitz, 2010: Regional precipitation trends: Distinguishing natural variability from anthropogenic forcing. *J. Climate*, **23**, 2131–2145, doi:10.1175/2009JCLI3420.1.

——, ——, ——, X.-W. Quan, K. Wolter, and L. Cheng, 2016: Characterizing recent trends in U.S. heavy precipitation. *J. Climate*, **29**, 2313–2332, doi:10.1175/JCLI-D-15-0441.1.

Huffman, G. J., R. F. Adler, D. T. Bolvin, and G. Gu, 2009: Improving the global precipitation record: GPCP version 2.1. *Geophys. Res. Lett.*, **36**, L17808, doi:10.1029/2009GL040000.

Hurrell, J. W., J. J. Hack, D. Shea, J. M. Caron, and J. Rosinski, 2008: A new sea surface temperature and sea ice boundary dataset for the Community Atmosphere Model. *J. Climate*, **21**, 5145–5153, doi:10.1175/2008JCLI2292.1.

Kay, J. E., and Coauthors, 2015: The Community Earth System Model (CESM) large ensemble project: A community resource for studying climate change in the presence of internal climate variability. *Bull. Amer. Meteor. Soc.*, **96**, 1333–1349, doi:10.1175/BAMS-D-13-00255.1.

Kent, C., R. Chadwick, and D. P. Rowell, 2015: Understanding uncertainties in future projections of seasonal tropical precipitation. *J. Climate*, **28**, 4390–4413, doi:10.1175/JCLI-D-14-00613.1.

Laepple, T., and P. Huybers, 2014: Global and regional variability in marine surface temperatures. *Geophys. Res. Lett.*, **41**, 2528–2534, doi:10.1002/2014GL059345.

Lamarque, J.-F., G. P. Kyle, M. Meinshausen, K. Riahi, S. J. Smith, D. P. Vuuren, A. J. Conley, and F. Vitt, 2011: Global and regional evolution of short-lived radiatively-active gases and aerosols in the representative concentration pathways. *Climatic Change*, **109**, 191–212, doi:10.1007/s10584-011-0155-0.

Liebmann, B., I. Bladé, G. N. Kiladis, L. M. V. Carvalho, G. B. Senay, D. Allured, S. Leroux, and C. Funk, 2012: Seasonality of African precipitation from 1996 to 2009. *J. Climate*, **25**, 4304–4322, doi:10.1175/JCLI-D-11-00157.1.

——, and Coauthors, 2014: Understanding recent eastern Horn of Africa rainfall variability and change. *J. Climate*, **27**, 8630–8645, doi:10.1175/JCLI-D-13-00714.1.

Lott, F. C., N. Christidis, and P. A. Stott, 2013: Can the 2011 East African drought be attributed to human-induced climate change? *Geophys. Res. Lett.*, **40**, 1177–1181, doi:10.1002/grl.50235.

Lyon, B., 2014: Seasonal drought in the Greater Horn of Africa and its recent increase during the March–May long rains. *J. Climate*, **27**, 7953–7975, doi:10.1175/JCLI-D-13-00459.1.

——, and D. G. DeWitt, 2012: A recent and abrupt decline in the East African long rains. *Geophys. Res. Lett.*, **39**, L02702, doi:10.1029/2011GL050337.

——, A. Barnston, and D. DeWitt, 2014: Tropical Pacific forcing of a 1998–1999 climate shift: Observational analysis and climate model results for the boreal spring season. *Climate Dyn.*, **43**, 893–909, doi:10.1007/s00382-013-1891-9.

Mantua, N. J., S. R. Hare, Y. Zhang, J. M. Wallace, and R. C. Francis, 1997: A Pacific interdecadal climate oscillation with impacts on salmon production. *Bull. Amer. Meteor. Soc.*, **78**, 1069–1079, doi:10.1175/1520-0477(1997)078<1069:APICOW>2.0.CO;2.

Meehl, G. A., and H. Teng, 2012: Case studies for initialized decadal hindcasts and predictions for the Pacific region. *Geophys. Res. Lett.*, **39**, L22705, doi:10.1029/2012GL053423.

——, A. Hu, and C. Tebaldi, 2010: Decadal prediction in the Pacific region. *J. Climate*, **23**, 2959–2973, doi:10.1175/2010JCLI3296.1.

——, and Coauthors, 2014: Decadal climate prediction: An update from the trenches. *Bull. Amer. Meteor. Soc.*, **95**, 243–267, doi:10.1175/BAMS-D-12-00241.1.

Meinshausen, M., and Coauthors, 2011: The RCP greenhouse gas concentrations and their extensions from 1765 to 2300. *Climatic Change*, **109**, 213–241, doi:10.1007/s10584-011-0156-z.

Newman, M., and Coauthors, 2016: The Pacific decadal oscillation, revisited. *J. Climate*, **29**, 4399–4427, doi:10.1175/JCLI-D-15-0508.1.

Otieno, V., and R. O. Anyah, 2013: CMIP5 simulated climate conditions of the Greater Horn of Africa (GHA). Part II: Projected climate. *Climate Dyn.*, **41**, 2099–2113, doi:10.1007/s00382-013-1694-z.

Pall, P., T. Aina, D. A. Stone, P. A. Stott, T. Nozawa, A. G. J. Hilberts, D. Lohmann, and M. R. Allen, 2011: Anthropogenic greenhouse gas contribution to flood risk in England and Wales in autumn 2000. *Nature*, **470**, 382–385, doi:10.1038/nature09762.

Perlwitz, J., M. Hoerling, J. Eischeid, T. Xu, and A. Kumar, 2009: A strong bout of natural cooling in 2008. *Geophys. Res. Lett.*, **36**, L23706, doi:10.1029/2009GL041188.

Roeckner, E., and Coauthors, 2006: Sensitivity of simulated climate to horizontal and vertical resolution in the ECHAM5 atmosphere model. *J. Climate*, **19**, 3771–3791, doi:10.1175/JCLI3824.1.

Shongwe, M. E., G. J. van Oldenborgh, B. van den Hurk, and M. van Aalst, 2011: Projected changes in mean and extreme precipitation in Africa under global warming. Part II: East Africa. *J. Climate*, **24**, 3718–3733, doi:10.1175/2010JCLI2883.1.

Sigmond, M., and J. C. Fyfe, 2016: Tropical Pacific impacts on cooling North American winters. *Nat. Climate Change*, **6**, 970–974, doi:10.1038/nclimate3069.

Solomon, A., and M. Newman, 2012: Reconciling disparate twentieth-century Indo-Pacific ocean temperature trends in the instrumental record. *Nat. Climate Change*, **2**, 691–699, doi:10.1038/nclimate1591.

Tanre, D., J.-F. Geleyn, and J. M. Slingo, 1984: First results of the introduction of an advance aerosol-radiation interaction in the ECMWF low resolution global model. *Aerosols and Their Climatic Effects*, H. E. Gerber and A. Deepak, Eds., A Deepak Publishing, 133–177.

Taylor, K. E., R. J. Stouffer, and G. A. Meehl, 2012: An overview of CMIP5 and the experiment design. *Bull. Amer. Meteor. Soc.*, **93**, 485–498, doi:10.1175/BAMS-D-11-00094.1.

Tierney, J. E., C. C. Ummenhofer, and P. B. deMenocal, 2015: Past and future rainfall in the Horn of Africa. *Sci. Adv.*, **1**, doi:10.1126/sciadv.1500682.

Verdin, J., C. Funk, G. Senay, and R. Choularton, 2005: Climate science and famine early warning. *Philos. Trans. Roy. Soc. London*, **360B**, 2155–2168, doi:10.1098/rstb.2005.1754.

Wilcox, L. J., E. J. Highwood, and N. J. Dunstone, 2013: The influence of anthropogenic aerosol on multi-decadal variations of historical global climate. *Environ. Res. Lett.*, **8**, 024033, doi:10.1088/1748-9326/8/2/024033.

Williams, A. P., and C. Funk, 2011: A westward extension of the warm pool leads to a westward extension of the Walker circulation, drying eastern Africa. *Climate Dyn.*, **37**, 2417–2435, doi:10.1007/s00382-010-0984-y.

Yang, W., R. Seager, M. A. Cane, and B. Lyon, 2014: The East African long rains in observations and models. *J. Climate*, **27**, 7185–7202, doi:10.1175/JCLI-D-13-00447.1.

Yeh, S.-W., Y.-G. Ham, and J.-Y. Lee, 2012: Changes in the tropical Pacific SST trend from CMIP3 to CMIP5 and its implication of ENSO. *J. Climate*, **25**, 7764–7771, doi:10.1175/JCLI-D-12-00304.1.

Zhang, Y., J. M. Wallace, and D. S. Battisti, 1997: ENSO-like interdecadal variability: 1900–93. *J. Climate*, **10**, 1004–1020, doi:10.1175/1520-0442(1997)010<1004:ELIV>2.0.CO;2.